NUKLEONIKA 2013;58(1):235–240

ORIGINAL PAPER

Ortho-positronium migration in mesopores of MCM-41, MSF and SBA-3

Radosław Zaleski,
Artur Błażewicz,
Agnieszka Kierys

Abstract. Three materials: MCM-41, MSF and SBA-3 with a very similar pore diameter but different lengths of cylindrical pores were investigated using the nitrogen sorption method and positron annihilation lifetime spectroscopy. The size of primary pores and interparticle spaces obtained by both methods is similar. However, volume ratios between the discussed kinds of pores found by the above-mentioned methods differ significantly. Such discrepancy is the result of both *ortho*-positronium migration and the inaccessibility of the pores for nitrogen. Comparing the results of nitrogen sorption and positron annihilation lifetime spectroscopy allows us to estimate that connectivity between the primary pores and the interparticle spaces is the highest in MCM-41 and lowest in SBA-3.

Key words: nitrogen adsorption/desorption • porous materials • positron annihilation lifetime spectroscopy (PALS) • positronium migration

R. Zaleski✉, A. Błażewicz
Maria Curie-Skłodowska University,
Institute of Physics,
Department of Nuclear Methods,
1 M. Curie-Skłodowskiej Sq., 20-031 Lublin, Poland,
Tel.: +48 81 537 6225, Fax: +48 81 537 6191,
E-mail: radek@zaleski.umcs.pl

A. Kierys
Maria Curie-Skłodowska University,
Faculty of Chemistry,
Department of Adsorption,
3 M. Curie-Skłodowskiej Sq., 20-031 Lublin, Poland

Received: 1 August 2012
Accepted: 26 September 2012

Introduction

Recent studies prove that positron annihilation lifetime spectroscopy (PALS) can be successfully used as a porosimetric technique [8, 11, 26–28]. PALS has several advantages over the standard sorption techniques, i.e., the range of PALS's sensitivity spreads over mesopores and micropores (reaching even the intermolecular free spaces of several angstroms [26]). It allows the characterization of closed pores [15, 20, 22] measurements can be performed in ambient temperatures or in any temperature range from 0 K to several hundred Kelvin [4, 12, 18, 30] and PALS measurements can be performed *in situ* (e.g. at various mechanical pressures [24] or in the presence of a pore filling gas [6, 21, 23]). Such features are impossible to obtain by the most popular sorption methods. However, PALS limitations are less known than the limitations of sorption methods. Therefore investigating the porosity of various materials is required to verify the positron porosimetry reliability. A comparison of the PALS results with findings from other methods gives the ability to find the phenomena influencing positron annihilation lifetime spectra, which have to be taken into account in order to obtain correct results or their proper interpretation. One of such phenomena is positronium migration.

Positron porosimetry consists in measurement of positronium lifetime. Positronium is a hydrogen-like bound state of a positron and an electron, which is formed randomly in the sample volume as a result of interaction between a positron emitted from a radioactive source and one of the electrons present in the sample.

Because the positronium singlet state *para*-positronium (*p*-Ps) annihilates with an average lifetime of 125 ps almost without any dependance on the material, the probe used for pore size characterization is the positronium triplet state *ortho*-positronium (*o*-Ps). It annihilates with a lifetime up to 142 ns in vacuum, which can be shortened to even below 1 ns due to the pick-off process. Pick-off consists in an annihilation of the positron bound in *o*-Ps with an electron from the material, instead of an annihilation with the electron bound in *o*-Ps. Assuming that *o*-Ps is trapped in the free volume of a certain size, the relation between the *o*-Ps lifetime and the size of the free volume is described by the extended Tao-Eldrup (ETE) model [3]. Usually, there are several fractions of positrons trapped in free volumes of different sizes. The relation between the intensity of *o*-Ps annihilating with a particular lifetime and the total volume of free spaces with a particular size may be also found [5, 25]. These relations allow the reconstruction of the distribution of pore sizes.

Unfortunately, *o*-Ps does not always annihilate in the free volume in which it was formed. If pores of different sizes are connected, it is possible that *o*-Ps forms in smaller pore and migrates to the larger one before it annihilates. In consequence, the *o*-Ps exists longer and annihilates with a lifetime characteristic of the size of the larger free volume. Whereas the intensity of the *o*-Ps fraction annihilating with this lifetime depends on the volume of smaller free pores (and the probability of the migration) instead of the volume of the larger pores, as it is assumed in the model described above. As a result, the apparent distribution of pore size is distorted. An opposite migration (i.e., from a larger pore to a smaller one) is also possible, but less probable, because it is energetically unfavourable; zero point energy level of *o*-Ps trapped in larger free volumes is lower than in the smaller ones. Therefore, it should play a significant role only at high temperatures, when excited levels occupation is significant.

In order to investigate the influence of *o*-Ps migration on the PALS results at room temperature three materials: MCM-41, SBA-3 and MSF were investigated. In each of them there were particles consisting of a hexagonal (honeycomb-like) structure of cylindrical pores (primary pore structure). The diameter of primary pores is similar in all materials, but there is a difference in their length. There are also interparticle free spaces, several times larger than primary pores present in the materials. Their contribution to the total pore volume cannot be neglected due to the fine size of the material grains. The different lengths of primary pores results in different connectivity between the primary pores and interparticle spaces. Therefore, a different probability of *o*-Ps migration in each of the materials is expected.

Experimental

Quanta™ 3D FEG operating at 30.0 kV was used to obtain the scanning electron microscopy micrographs.

Nitrogen adsorption and desorption isotherms at 77 K were measured using the Quantachrome 1CMS Autosorb. The specific surface area (*S*) of the sample was determined using the Brunauer-Emmet-Teller (BET) method in the relative pressure p/p_0 range 0.05–0.3. The total pore volume (*V*) was assumed to be equal to the volume of nitrogen adsorbed at a relative pressure of about 0.99. Porosity of the sample (*P*) was calculated assuming density of the walls equal to the density of amorphous silica 2.2 g/cm^2 [19]. Pore size distributions were calculated using the Barrett-Joyner-Halenda (BJH) method [1] by a Quantochrome Autosorb 1.51 software.

A standard fast-slow delayed coincidence spectrometer equipped with BaF_2 scintillators was used for the positron lifetime measurements. An 80 kBq ^{22}Na isotope sealed between two 8 μm thick layers of Kapton foil served as the positron source. The source was placed between two 2 mm thick layers of samples and such a "sandwich" was put inside a vacuum chamber. Initially, all samples were in the form of fine powder. In order to keep the same sample structure during PALS and nitrogen sorption measurements the sample was loosely put into the sample holder and closed by a gently twisted cap. The chamber was evacuated to 10^{-3} Pa to avoid the positronium *ortho-para* conversion caused by oxygen. Moreover, it allowed us to remove most of the adsorbed gases and water from the sample surface. PALS measurements for each sample were performed in a temperature range from 93 K to 373 K with a 20 K step. Application of a Shimaden MR13 PID controller allowed us to obtain a stability of temperature within an 0.2 K range. The rate of coincidence registration was about 1.5×10^6 per hour. The measurement at each temperature lasted for 10 h. The resolution curve was approximated by two Gaussians (83% and 17% contribution) with the resultant FWHM (full width at half maximum) equal to 0.31 ns. Numerical analyses of the spectra were performed using the MELT routine [16].

Materials

Mesoporous silica MCM-41 was prepared using a cationic surfactant hexadecyltrimethylammonium bromide (CTAB, 98%, Sigma) as a template and tetraethyl orthosilicate (TEOS, 98%, Aldrich) as a silica source. The detailed synthesis was described elsewhere [7]. In brief, 2.4 g of the surfactant was dissolved in 120 g of distilled water, and subsequently 9.5 g of 25 wt.% NH_4OH was introduced. Subsequently, 10 g of TEOS was dropped slowly into a surfactant solution. The preparation procedure of SBA-3-type mesoporous sieve followed the method described SBA-3 type in the literature [2, 9]. Briefly, 2.4 g of CTAB and 43 g of HCl (37 wt.%) were dissolved in 112 g of de-ionized water while stirring. Next, 10 g of TEOS was added dropwise to the CTAB solution.

Mesoporous silica fibres MSF were prepared using tetrabutyl orthosilicate (TBOS, 97%, Aldrich) as a silica source. The MSF synthesis was based on the procedure described in Refs. [10, 13, 14]. The acidic surfactant solution was prepared by dissolving 5.61 g of CTAB and 181 g of HCl (37 wt.%) in 1123 g of de-ionized water. Then, 10 g of TBOS was added without stirring to form a thin layer on the top of the CTAB aqueous solution. The two-phase solution was aged for 10 days at room temperature.

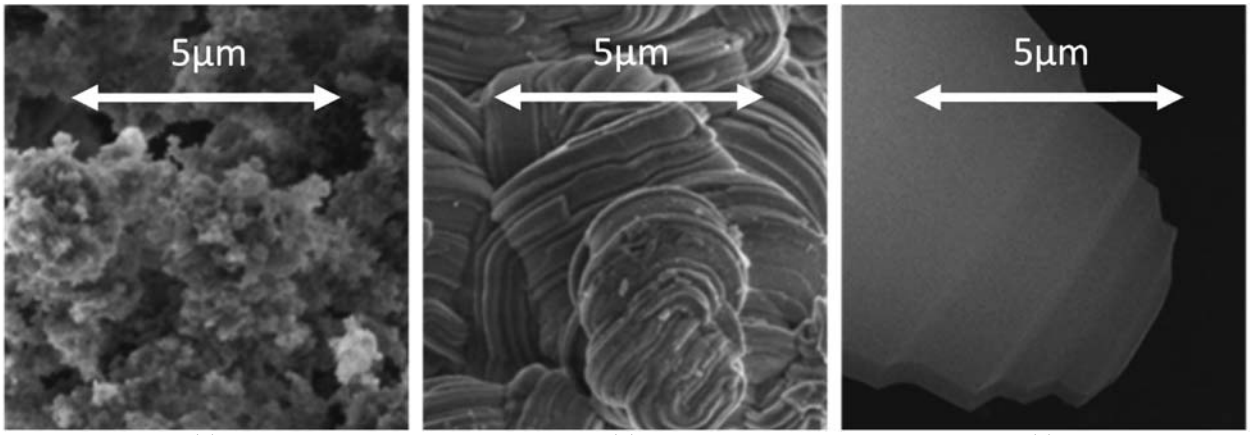

Fig. 1. Scanning electron microscopy micrographs of MCM-41 (a), SBA-3 (b) and MSF (c).

Table 1. Total pore volume (V), specific surface area (S) and porosity (P) of MCM-41, MSF and SBA-3 samples calculated from results of low temperature nitrogen adsorption/desorption

	V (cm^3/g)	S (m^2/g)	P (%)
MCM-41	0.95	1163	68
MSF	0.72	1234	61
SBA-3	0.59	1320	57

The as-synthesized samples, i.e. MCM-41, SBA-3 and MSF, were filtered, washed with 3 l of distilled water and dried at 100°C for 6 h. Finally, after calcination at 550°C for 6 h, the resultant template-free silicas were obtained. The results of samples characterization by the nitrogen sorption method is given in Table 1.

Results and discussion

Scanning electron microscopy images (Fig. 1) show the structure of MCM-41, SBA-3 and MSF grains. These images allow us to estimate the length of the pores and their connectivity to interparticle spaces. The grains of MCM-41 are definitely the smallest. Their jagged shape suggests short primary pores (several hundred nanometers at most) and a high connectivity between them and the interparticle spaces. Particles of SBA-3 are much denser. Bundles of pores seem to have a length of several micrometers and are often bent instead of having an open end. Their connectivity with interparticle spaces seems to be much worse than in the case of MCM-41. MSF has an even more compact structure. Primary pores are usually toroidal and form fiber-like grains where the plane in which the toroids are formed is perpendicular to the fiber symmetry axis. In such a structure no connectivity between the primary pores and interparticle spaces is expected. However, one has to remember that during the template removal, products of thermal surfactant decomposition had to find or create their way outside the primary pores. Therefore, the existence of holes in the primary pore walls is suspected.

However, nitrogen adsorption/desorption isotherms of MSF (Fig. 2) do not confirm a higher concentration of micropores than in other samples, which is suspected as a result of the template removal from closed pores. Moreover, it is very surprising that the shape of isotherms of all investigated samples is similar in the range of $p/p_0 < 0.2$. Unlike other samples, MSF is characterized by the higher nitrogen adsorption in a p/p_0 range of 0.2–0.3. This may suggest that the pores located in the pore walls are relatively large, comparable to the size of primary pores. The MCM-41 nitrogen isotherm is of type IV, according to the IUPAC nomenclature [17], indicating the presence of mesopores. A narrow step with a negligible hysteresis at $p/p_0 = 0.3$, characteristic of equally sized primary pores, is visible. At the same time isotherms of both the SBA-3 and MSF materials do not exhibit any presence of a hysteresis loop, which is unexpected. However, it is rather the result of nitro-

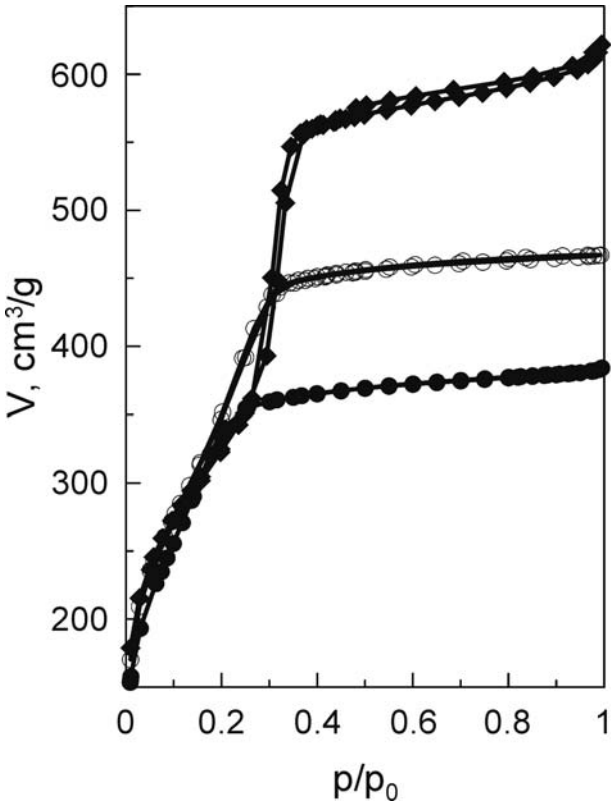

Fig. 2. Low-temperature nitrogen adsorption and desorption isotherms of MCM-41 (diamonds), SBA-3 (circles) and MSF (empty circles).

Table 2. Lifetimes at the maximum of the distribution and component intensities for MCM-41, SBA-3 and MSF samples

	o-Ps lifetimes (ns)			
	τ_3	τ_4	τ_5	τ_6
MCM-41	2.7	11.1	35.7	120.1
MSF	1.9	10.7	40.5	123.4
SBA-3	3.5	14.4	32.5	118.8
	o-Ps intensities (%)			
	I_3	I_4	I_5	I_6
MCM-41	0.9 ± 0.3	1.2 ± 0.2	4.5 ± 0.2	20.6 ± 0.2
MSF	1.2 ± 0.3	1.0 ± 0.2	17.3 ± 3.6	7.7 ± 3.5
SBA-3	1.2 ± 0.3	2.2 ± 1.1	24.8 ± 1.0	5.2 ± 0.2

gen being unable to access the mesopores due to a low connectivity between the primary pores and interparticle spaces, than the absence of the primary pores. Assuming that the amount of nitrogen adsorbed at $p/p_0 >$ 0.3, where it is almost constant, reflects the connectivity between the primary pores and interparticle spaces, we can estimate that the highest connectivity is present in MCM-41, and the lowest one in SBA-3.

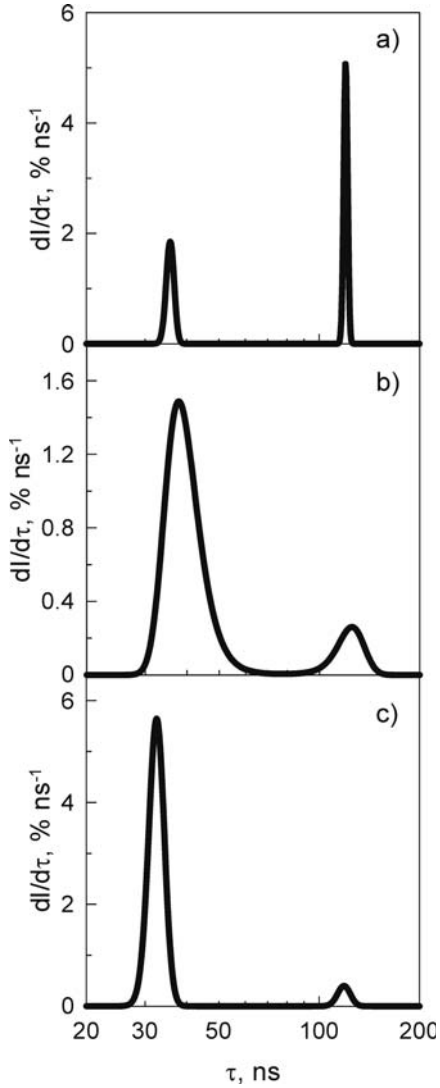

Fig. 3. Intensity histograms for the two long-lived *o*-Ps components obtained by the MELT analysis of positron annihilation lifetime spectra measured at 293 K for MCM-41 (a), MSF (b) and SBA-3 (c).

Analyses of PALS spectra performed using MELT revealed six components in each sample. Their origins are *p*-Ps (0.12–0.15 ns), unbound positrons (0.5–0.6 ns) and four fractions of *o*-Ps (Table 2). Unfortunately, the form of results obtained by MELT (histogram of lifetimes) allow only to determine uncertainty of intensities. The lifetimes at the maximum given in Table 2 indicate only histogram maxima. Therefore, it has to be noticed that parameters (Fig. 3) of the third and fourth component are determined only approximately, because their intensities are relatively low. *Ortho*-positronium fractions can be ascribed to annihilation in a silica skeleton (τ_3), micropores (τ_4), mesopores (τ_5) and interparticle spaces (τ_6). The lifetimes of particular components (τ_3–τ_6) and the intensities of the two short-lived *o*-Ps components (I_3, I_4) are close to each other in all samples. The only significant differences between the samples are observed in intensities of the two long-lived *o*-Ps components (I_5, I_6). In MCM-41 the intensity of the interparticle spaces component I_6 predominates over the intensity of the primary pores component I_5, while in the other samples an opposite tendency is observed. The simplest explanation is that in MCM-41 there exists a larger volume of interparticle spaces as compared to other investigated samples. However, a study of MCM-41 with the primary pores filled by template [29, 30] allows us to estimate the intensity of *o*-Ps formed in interparticle spaces only, which is three times smaller than after the template removal. Therefore, the most probable explanation of the small ratio of $I_5/I_6 = 0.2$ in MCM-41 is the migration of *o*-Ps formed in primary pores, which are very short, to the interparticle spaces. Whereas, such a process is less probable in MSF, where $I_5/I_6 = 2.2$, and even less probable in SBA-3 ($I_5/I_6 = 4.8$).

In order to verify the idea of *o*-Ps migration, pore size distributions obtained from PALS spectra were compared to the ones derived from the low-temperature nitrogen adsorption/desorption data using BJH calculations (Fig. 4). While there is a good agreement between pore size distributions in a range of several nanometers (i.e., primary pores), there is a very small contribution of interparticle spaces in pore size distributions derived from nitrogen adsorption/desorption. Quantitative data are presented in Table 3, where the volume of primary pores V_p was calculated for pores with size D = 1.7–5 nm, and volume of interparticle spaces V_i – for pores with size $D > 5$ nm. The data have an approximate character, as both methods have hard to estimate uncertainty. The data shows that, accord-

Table 3. Relative volume of primary pores (V_p), interparticle spaces (V_i) and the ratio of interparticle spaces volume to total mesopore volume obtained from distributions calculated from nitrogen adsorption/desorption isotherms (left) and PALS spectra (right) for MCM-41, SBA-3 and MSF samples

	LN_2			PALS		
	V_p (cm³/g)	V_i (cm³/g)	$V_i/(V_p + V_i)$ (%)	V_p (a.u.)	V_i (a.u.)	$V_i/(V_p + V_i)$ (%)
MCM-41	0.88	0.063	7	0.046 ± 0.002	0.207 ± 0.002	82 ± 1
MSF	0.69	0.016	2	0.17 ± 0.04	0.07 ± 0.03	29 ± 14
SBA-3	0.33	0.024	7	0.25 ± 0.01	0.051 ± 0.002	17 ± 1

ing to nitrogen adsorption/desorption, contribution of interparticle spaces does not exceed several percent of the total mesopore volume. The smallest contribution was found for MSF, which is quite reasonable because of the compact structure of this fibre-like material. In contrary, contributions of interparticle spaces calculated from pore size distributions obtained by PALS data are several times larger. These values are most likely distorted due to the positronium migration, the probability of which is largest in MCM-41 and smallest in SBA-3. This result is in agreement with the previously presented estimations of connectivity between both kinds of free volumes based on nitrogen adsorption/desorption isotherms. Nevertheless, it should be noticed that the results of both methods, nitrogen sorption and PALS, may be distorted due to a different connectivity of the pores in an opposite way. Nitrogen does not penetrate some of the smaller pores if they are poorly connected to outer spaces, while positronium escapes from smaller pores if their connectivity is good.

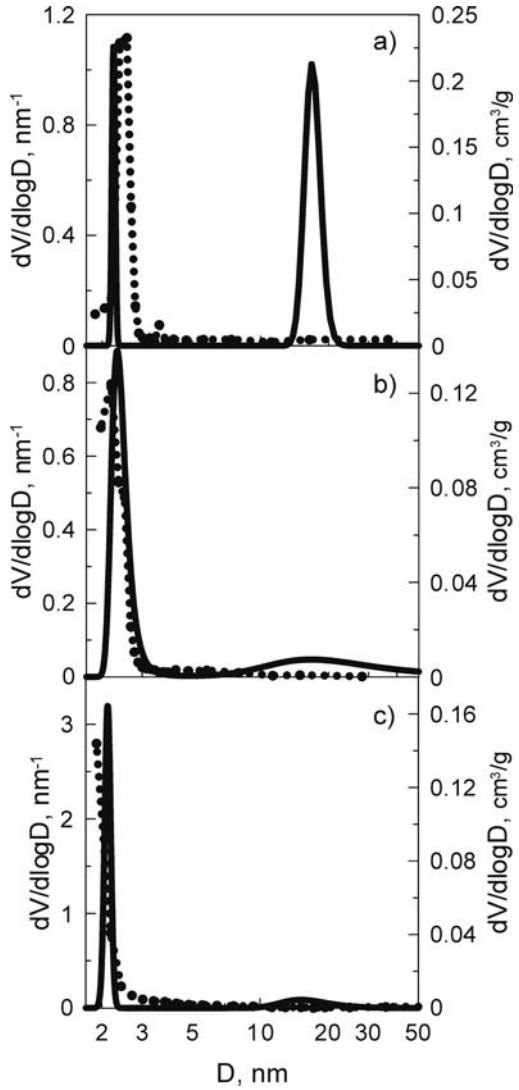

Fig. 4. Pore size distributions derived from low-temperature nitrogen adsorption/desorption data using the BJH calculations (dotted line) and from PALS spectra using the ETE model and the relation between the intensity and pore volume (solid line) for MCM-41 (a), MSF (b) and SBA-3 (c).

Another effect caused by positronium migration, which should be expected, is the shortening of τ_5 (migration probability is added to the pick-off decay constant). It can be found in Fig. 4 that the pore size calculated from the fifth component lifetime distribution is smaller than expected from the BJH calculations only in MCM-41. In other distributions there is an opposite tendency. It may be the result of greater lifetime shortening due to a more probable *o*-Ps migration in MCM-41 in comparison to other samples. However, this does not explain the larger than expected lifetimes in MSF and SBA-3. In these cases pore sizes may be underestimated by liquid nitrogen sorption due to a poor accessibility of the pores. Unfortunately, the size of primary pores is close to the lower limit of BJH applicability and results of this method are not accurate.

Conclusions

Modern materials with tailored not only pore size but also pore length and their connectivity allow us to verify the results of techniques used for porosity characterization. It is especially important in the case of positron porosimetry based on PALS. Development of the technique of pore characterization requires verification of the results and, as a consequence, improvement of calculation methods used for determination of pore size distribution. Presented findings show that one of the effects that has to be taken into account is the migration of *o*-Ps. Comparison of nitrogen sorption and PALS results shows a discrepancy in the derived ratio between the volume of primary pores and interparticle spaces between these techniques. It is the result of *o*-Ps migration, probability of which is different in each material. The differences between both methods may reveal a degree of connectivity between primary pores and interparticle spaces. The highest connectivity was found for MCM-41 and the lowest one – for SBA-3.

The connectivity between primary pores and interparticle spaces influences not only the PALS results, but also the nitrogen sorption results. Nitrogen sorption is more reliable for short and open pores, while PALS results are more accurate for closed or at least very long pores. Moreover, for short pores, when migration is highly probable, the lifetime measured by PALS is

shortened, distorting the pore size estimated using the ETE model. Because both PALS and nitrogen sorption are sensitive to pore connectivity in opposite ways, they can provide complementary results. Particularly interesting is the possibility to estimate pore connectivity or their length using these combined methods.

Acknowledgment. This work was supported by the Polish Ministry of Science and Higher Education Grant No. N N204 131137.

References

1. Barrett EP, Joyner LG, Halenda PP (1951) The determination of pore volume and area distributions in porous substances. I. Computations from nitrogen isotherms. J Am Chem Soc 73;1:373–380
2. Chen F, Xu X-J, Shen S, Kawi S, Hidajat K (2004) Microporosity of SBA-3 mesoporous molecular sieves. Microporous Mesoporous Mater 75;3:231–235
3. Ciesielski K, Dawidowicz AL, Goworek T, Jasińska B, Wawryszczuk J (1998) Positronium lifetimes in porous Vycor glass. Chem Phys Lett 289;1/2:41–45
4. Fischer CG, Weber MH, Wang CL, McNeil SP, Lynn KG (2005) Positronium in low temperature mesoporous films. Phys Rev B 71;18:180102
5. Gidley DW, Frieze WE, Dull TL *et al*. (2000) Determination of pore-size distribution in low-dielectric thin films. Appl Phys Lett 76;10:1282–1284
6. Goldanskii V, Mokrushin A, Tatur A, Shantarovich V (1975) Positronium interactions with gases in pores of silicagels. Appl Phys A 5;4:379–382
7. Grün M, Unger KK, Matsumoto A, Tsutsumi K (1997) Ordered mesoporous MCM-41 adsorbents: novel routes in synthesis, product, characterization and specification. In: McEnaney B, Mays JT, Rouquerol J, Rodriguez-Reinoso F, Sing KSW, Unger KK (eds) Characterisation of porous solids IV. Royal Society of Chemistry, Cambridge, p 81
8. He C, Suzuki R, Ohdaira T *et al*. (2007) Study of mesoporous silica films by positron annihilation based on a slow positron beam: Effects of preparation conditions on pore size and open porosity. Chem Phys 331;2/3:213–218
9. Huo Q, Margolese DI, Stucky GD (1996) Surfactant control of phases in the synthesis of mesoporous silica-based materials. Chem Mater 8;5:1147–1160
10. Huo Q, Zhao D, Feng J *et al*. (1997) Room temperature growth of mesoporous silica fibers: A new high-surface--area optical waveguide (abstract). ChemInform 28:48
11. Kullmann J, Enke D, Thraenert S, Krause-Rehberg R, Inayat A (2010) Characterization of nanoporous monoliths using nitrogen adsorption and positronium annihilation lifetime spectroscopy. Colloids Surf A 357;1/3:17–20
12. Kunishige S, Koshimizu M, Asai K (2009) Temperature dependence of positron lifetime in ordered porous silica (SBA-3). Radiat Phys Chem 78;12:1088–1091
13. Marlow F, Kleitz F (2001) Mesoporous silica fibers: internal structure and formation. Microporous Mesoporous Mater 44/45:671–677
14. Marlow F, McGehee MD, Zhao D, Chmelka BF, Stucky GD (1999) Doped mesoporous silica fibers: A new laser material. Adv Mater 11;8:632–636
15. Petkov MP, Wang CL, Weber MH, Lynn KG, Rodbell KP (2003) Positron annihilation techniques suited for porosity characterization of thin films. J Phys Chem B 107;12:2725–2734
16. Shukla A, Peter M, Hoffmann L (1993) Analysis of positron lifetime spectra using quantified maximum entropy and a general linear filter. Nucl Instrum Methods Phys Res A 335;1/2:310–317
17. Sing KSW, Everett DH, Moscou RAWL, Pierotti RA, Rouquerol J, Siemieniewska T (1985) Reporting physisorption data for gas/solid systems with special reference to the determination of surface area and porosity (Recommendations 1984). Pure Appl Chem 57;4:603–619
18. Thraenert S, Hassan EM, Enke D, Fuerst D, Krause--Rehberg R (2007) Verifying the RTE model: ortho--positronium lifetime measurement on controlled pore glasses. Phys Status Solidi C 4;10:3819–3822
19. Ustinov EA, Do DD, Jaroniec M (2005) Adsorption of argon and nitrogen in cylindrical pores of MCM-41 materials: application of density functional theory. Appl Surf Sci 252;4:1013–1028
20. Wang CL, Weber MH, Lynn KG, Rodbell KP (2002) Nanometer-scale pores in low-k dielectric films probed by positron annihilation lifetime spectroscopy. Appl Phys Lett 81;23:4413–4415
21. Wilkinson NJ, Alam MA, Clayton JM, Evans R, Fretwell HM, Usmar SG (1992) Positron annihilation study of capillary condensation of nitrogen gas in a mesoporous solid. Phys Rev Lett 69;24:3535–3538
22. Xi-Jie D, Yi-Fan H, Yu-Ying W (2010) Positronium diffusion in porous methylsilsesquioxane thin films. Chin Phys B 19;1:013601
23. Zaleski R, Dolecki W, Kierys A, Goworek J (2012) n-Heptane adsorption and desorption on porous silica observed by positron annihilation lifetime spectroscopy. Microporous Mesoporous Mater 154:142–147
24. Zaleski R, Goworek J, Borówka A, Kierys A, Wiśniewski M (2009) Positron porosimetry study of mechanical stability of ordered mesoporous materials. In: Seaton N, Reinoso FR, Llewellyn P, Kaskel S (eds) Characterisation of porous solids VIII. RSC Publishing, Cambridge, pp 400–407
25. Zaleski R, Goworek J, Maciejewska M (2009) Positronium lifetime in porous VP-DVB copolymer. Phys Status Solidi C 6;11:2445–2447
26. Zaleski R, Kierys A, Dziadosz M, Goworek J, Halasz I (2012) Positron annihilation and N2 adsorption for nanopore determination in silica-polymer composites. RSC Advances 2;9:3729–3734
27. Zaleski R, Kierys A, Grochowicz M, Dziadosz M, Goworek J (2011) Synthesis and characterization of nanostructural polymer-silica composite: Positron annihilation lifetime spectroscopy study. J Colloid Interface Sci 358;1:268–276
28. Zaleski R, Stefaniak W, Maciejewska M, Goworek J (2010) Porosity evolution of VP-DVB/MCM-41 nanocomposite. J Colloid Interface Sci 343;1:134–140
29. Zaleski R, Wawryszczuk J (2008) Positron porosimetry studies of template removal from as-synthesized MCM-41 silica. Acta Phys Pol A 113;5:1543–1550
30. Zaleski R, Wawryszczuk J, Goworek J, Borówka A, Goworek T (2003) Vacuum removal of the template in MCM-41 silica studied by the positron annihilation method. J Colloid Interface Sci 262;2:466–473